



# Nonlinear waveform steepening in time reversal focusing of airborne, one-dimensional sound waves

Michael M. Hogg, 1 Brian D. Patchett, 1,2 and Brian E. Anderson 1,a) a

<sup>1</sup>Acoustics Research Group, Department of Physics and Astronomy, Brigham Young University, Provo, Utah 84602, USA

#### **ABSTRACT:**

Time reversal (TR) is a process that can be used to generate high amplitude focusing of sound. It has been previously shown that high amplitude focused sound using TR in reverberant environments exhibits multiple nonlinear features including waveform steepening and a nonlinear increase in peak compression pressures [Patchett and Anderson, J. Acoust. Soc. Am. 151(6), 3603–3614 (2022)]. The present study investigates the removal of one possible cause for these phenomena: free-space Mach stems. By constraining the focusing in the system to one-dimensional (1-D) waves, the potential formation of Mach stems is eliminated so that remaining nonlinear effects can be observed. A system of pipes is used to restrict the focused waves to be planar in a 1-D reverberant environment. Results show that waveform steepening effects remain, as expected, but that the nonlinear increase in compression amplitudes that appears in TR focusing of three-dimensional (3-D), finite-amplitude sound in rooms disappears here because Mach stems cannot form in a 1-D system. These experiments do not prove that Mach stems cause the nonlinear increase observed for focusing in a 3-D environment, but they do support the Mach stem explanation.

© 2025 Acoustical Society of America. https://doi.org/10.1121/10.0039638

(Received 22 April 2025; revised 10 September 2025; accepted 1 October 2025; published online 17 October 2025)

[Editor: Mark F. Hamilton] Pages: 3097–3106

#### I. INTRODUCTION

Time reversal (TR) is a signal processing technique that can be used to focus physical waves, acoustic or otherwise, to a selected spatial location in a system and provide temporal reconstruction. 1-4 Historically, acoustic TR was first used as a method to create localized and reproduceable underwater communications<sup>5,6</sup> that were difficult to intercept. More recent studies in communications have shown that TR allows for long distance communication in an ocean environment<sup>7,8</sup> and communication in among a network of pipes. Other uses for TR involve source localization in which waves propagate back through the environment to their original emission location. 10-12 There is also high amplitude focusing of sound and vibration, which is the main use of TR that the present study is concerned with.4 Studies of high amplitude focusing have investigated localized delivery of energy for many purposes, including nondestructive evaluation to find cracks<sup>3,13,14</sup> or to evaluate a structure's response to sound, 15-17 nonsurgical biomedical treatment, 18-20 and focusing sound loud enough to study nonlinear features in that focused sound.<sup>21–23</sup>

TR focusing relies on obtaining the impulse response (IR) from a source to a receiver. In a reverberant environment, the energy emitted from an impulsive emission takes many paths to the receiver. The arrival times of the reflections about the room are thus encoded in the IR. If this IR is time reversed and broadcast from the source, the paths that

were initially traversed, when the IR was obtained, are retraced such that energy simultaneously arrives at the receiver location from all of these paths. These simultaneous arrivals constructively interfere, resulting in high amplitude focusing of sound at the receiver location. In a reverberant environment, arrivals can come from all directions, resulting in an approximately converging spherical wave<sup>24</sup> made up of many diverging spherical waves (an expression of Huygen's principle). Multiple sources may be used in TR, and when their reversed IRs are synchronously timed, the amplitude of the focus is further increased.

As waves are being focused using TR, they are relatively low in amplitude before they converge at the focal location. However, at the focal location, whose spatial extent is roughly one wavelength in diameter, the peak amplitude can be three times higher on average than the amplitude of the converging waves. Thus, nonlinear features are more likely to be observed at the focal location than in the converging waves prior to focusing. This phenomenon is exploited when TR is used for nondestructive evaluation applications since the focusing is localized, and when the focusing occurs at a location on a sample that vibrates nonlinearly (i.e., a crack or delamination), then more nonlinearity may be observed in focusing at that location than when focusing at other intact locations on a sample. 14,25-27 Wallace and Anderson<sup>28</sup> showed that localized high amplitude focusing of two ultrasound frequencies in air could create an audible difference frequency. In biomedical ultrasound applications, waves focused with TR can generate localized heating at the focal location and be used to

<sup>&</sup>lt;sup>2</sup>Department of Physics, Utah Valley University, Orem, Utah 84058, USA

a)Email: bea@byu.edu

destroy kidney stones and brain tumors. <sup>18–20</sup> There are other ways to create high intensity focused ultrasound (HIFU) for biomedical applications besides using TR. In HIFU experiments and modeling, an increase in compression amplitudes and a decrease in rarefaction amplitudes has been observed, <sup>29</sup> but the physical mechanism was not explained.

Two nonlinear features have been asserted to happen during high amplitude TR focusing, waveform steepening and Mach stem formation. 22,23 In nonlinear acoustics, waveform steepening is due to an increase in wave speed in the compressions of the wave and a decrease in speed in the rarefactions of the wave as it propagates; both of which are breakdowns of the linear acoustics assumptions.<sup>30</sup> Thus, sine waves evolve toward sawtooth waveforms with shocks present where the slope of the waveform is nearly infinite.<sup>31</sup> When wave steepening occurs, the peak compression amplitudes are reduced relative to linear scaling as the wave continues to propagate. This feature causes a shifting of energy from the fundamental frequency to higher harmonics as the waveform steepens. Several authors 32-38 have provided experimental measurements that have been done in plane wave tubes to show wave steepening of sine waves and shock wave coalescence with noise waveforms; good agreement with weak shock theory (with the inclusion of tube wall losses) has been demonstrated. Mach stems form when high pressure wave fronts interfere and interact with one another. 23,39-42 One finite amplitude wave leaves behind excess heat in the medium (a breakdown of the adiabatic assumption), thereby increasing the sound speed in the medium behind it, and this increase in speed allows a trailing wave to catch up to the leading wave. This means Mach stems are typically observed in two-dimensional and threedimensional (3-D) environments where these types of interactions can occur. Unlike wave steepening, the compression amplitude in a Mach stem nonlinearly increases, producing pressures that are larger than the linear sum of the two constituent waves.

Montaldo et al. 43 reported data that exhibited nonlinear behavior in high amplitude TR focusing of ultrasound in a lithotripsy application. In their setup, as pulse excitation voltage was increased, the resulting focal signal exhibited increasing levels of nonlinearity, particularly waveform steepening, but not nonlinear amplification. Willardson et al.<sup>21</sup> reported nonlinearities in high amplitude TR focusing of audible frequency sound in a reverberation chamber, with a nonlinear increase in peak pressure in higher input amplitudes. They contrasted their results with those of Montaldo et al. and pointed out that the results reported by Montaldo et al. show a nonlinear decrease in compressions; nonlinearity was not discussed by Montaldo et al. Patchett and Anderson<sup>22</sup> furthered the work of Willardson et al. and created a peak focal pressure in air of 214.8 kPa or 200.6 dB<sub>peak</sub>. This amplitude was approximately two times higher than linear scaling would have predicted.<sup>22</sup> They also compared using eight individual loudspeakers to create eight focal signals and summing those in post processing to the case where all eight loudspeakers are used simultaneously, and it was clear that the nonlinear features were much more dramatic when all eight were used simultaneously.<sup>22</sup> Willardson et al.21 and Patchett and Anderson22 cite wave steepening as a possible contributing factor in their results. Patchett and Anderson further claim that free-space Mach stem formation is the mechanism of the nonlinear increase shown in the high amplitude compressions. This later claim was more fully studied by Patchett et al., 23 where they used numerical modeling to show that free-space Mach stem formation occurs in high amplitude TR when the high-pressure waves are allowed to interact. More information about Patchett's work can be found in Ref. 44. They also showed that when the TR focusing comes from a limited aperture (i.e., from a limited range of angles of incidence) that the nonlinear increase from Mach stems does not happen. This explains why it did not happen in the results reported by Montaldo et al. where waves in their setup converged from a limited aperture, but they were not constrained to propagate as plane waves in a waveguide. What is currently unknown is if a nonlinear increase would be observed in a system where wavefronts cannot overlap, meaning a case where Mach stems cannot form.

The purpose of this paper is to experimentally show that in a system in which waves are constrained to travel in one dimension, where Mach stems cannot form, that nonlinear amplification of peak compressions no longer happens. Thus, the observed nonlinearity that remains appears to be limited solely to waveform steepening. TR focusing experiments conducted in a room with waves converging in three dimensions are compared to TR focusing experiments conducted in a network of pipes with sound waves restricted to converge in one dimension. The bandwidth used for both sets of experiments, of 500–3500 Hz, restricts wave propagation to plane waves within the pipes. Experiments in both acoustic systems are conducted at sound levels where finite-amplitude, nonlinear effects are observed.

#### II. EXPERIMENTAL SETUP

The measurements for this study took place within a system of pipes. The pipes are made of cast iron, which should ensure very little excitation of pipe wall vibration due to the acoustic pressure waves. Waves inside the pipes reflect off of hard wall boundaries, and the only losses come from propagation (e.g., molecular relaxation) and thermoviscous boundary losses. Thus, the internal environment is considered reverberant albeit with a reverberation time of  $75 \pm 4.5$  ms. The pipes have a 5.08 cm (2 in.) inner diameter and were connected by various pieces that accommodate junctions of two, three, or four pipes in total. These junction pieces are referred to as couplers, T-pieces, and cross-pieces. In conjunction with various lengths of pipe, right BMS (Hannover, Germany) 4590 dual-diaphragm, high-output loudspeakers are fitted with appropriate crossover circuits and bolted to the ends of the pipes with flanges. Figure 1 shows a photograph of the actual system of pipes and loudspeakers used for the experiment. At the ends of each of the branches are the loudspeakers

previously mentioned. Notice that the lengths of the branches of the system are varied to prevent the formation of degenerate modes and to spread out the timing of reflections arriving at the microphone. Cross-modes and resonances may be generated in the junctions and bends in the pipes, but these waves evanesce as they travel away from the junction/bend and only plane waves emerge. Plane waves may be reflected by junctions and bends and the transmitted plane wave may be attenuated by traveling through the junction/bend, but only plane waves should exist when the sound field is measured a few duct diameters away from a junction or bend. Ar,48

An important feature of the pipe system is the straight section in the middle which is meant to let the plane waves propagate a distance in only a single duct before arriving at the microphone, a GRAS (Holte, Denmark) 46BG. This microphone was placed fully inside the pipe with its diaphragm located at the center of the pipe's cross section and also midway along the length of this linear section. The authors wanted to avoid having a flush mounted microphone that may rattle against the pipe walls. The microphone was kept in the center of the pipe via some foam and supporting structures. The wire connected to the microphone exited the pipe through a hole in the pipe wall, which was sealed with putty.

The TR process was carried out via a custom LABVIEW (National Instruments<sup>TM</sup>, Austin, TX) executable program developed in-house, <sup>49</sup> coupled with two Spectrum Instrumentation (Großhansdorf, Germany) M2i.6022 signal generation cards and an M2i.4931 digitizer card. The signals from the cards are output to two Crown (Elkhart, IN) CT4150 amplifiers, which send the signal to

the loudspeakers. Classical TR processing (simply broadcasting a band limited, time reversed impulse response (TRIR) with no coda compensation; more details in the following) is used in this study since we can see the nonlinearities without using the clipping TR method used by Patchett and Anderson.<sup>22</sup> We briefly explored focusing at even higher amplitude levels than those reported here (clipping TR was used as well) and found some strange amplitude dependent effects that were hard to explain, and we decided that these strange observations were setup specific (e.g., possibly caused by the microphone rattling against its supports and/or placing the microphone too close to a pipe end) and, thus, were not further explored.

To guarantee one-dimensional (1-D) propagation of waves in the system, the bandwidth of frequencies used in these experiments was limited to those below the plane wave tube cutoff frequency. The plane wave cutoff frequency for a circular duct is given by<sup>50</sup>

$$f_c = \frac{1.841c}{2\pi a},$$
 (1)

where c is the speed of sound, and a is the radius of the duct. For our system, we decided to limit our bandwidth to below 3500 Hz, which is well below  $f_c$  (approximately 3950 Hz) and used that as our maximum input frequency. A swept sine wave signal, or chirp signal, was created as the input signal to the system. A bandwidth of 500–3500 Hz was used to generate the chirp signal, with the lower frequency being determined by the limitation of the drivers themselves. Note that Golightly  $et\ al.^{51}$  also conducted TR

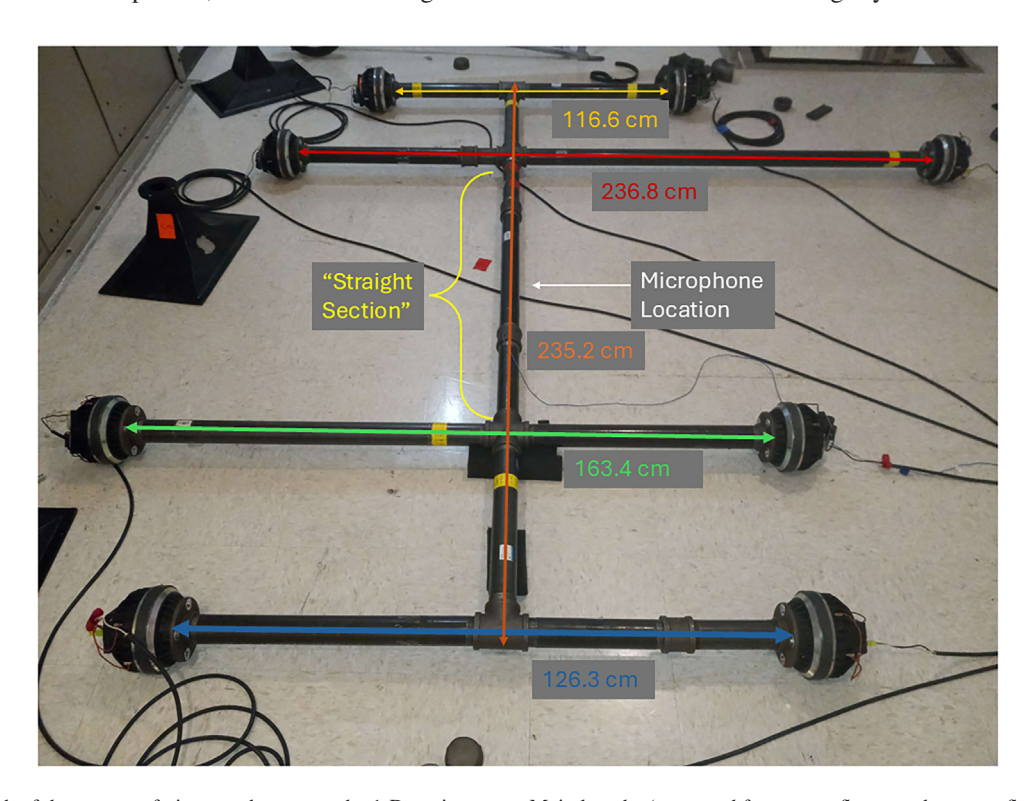


FIG. 1. Photograph of the system of pipes used to create the 1-D environment. Main lengths (measured from outer flange end to outer flange end) and locations are labeled.

experiments with plane waves in pipes but restricted their study to much lower sound levels for the purpose of exploring a super resolution concept.

The specific TR process that we use for these measurements is reciprocal TR,<sup>2</sup> which consists of a forward step and a backward step. During the forward step, a chirp signal [shown in Fig. 2(a)] is broadcast into the system from each driver, individually in turn. The microphone records the response of the system from each of the sources; these data are known as the chirp response (CR) [example also shown in Fig. 2(a)]. A cross correlation is performed between the chirp signal and the CR, resulting in an IR of the system. 52,53 This IR is then reversed in time to produce the TRIR [example shown in Fig. 2(b)]. During the backward step, the TRIR signals are simultaneously broadcast from all sources into the system. The direct propagation delay from the source and timing of reflections that arrive at the microphone are encoded into the TRIR and upon broadcast of the TRIR, energy will partially retrace these paths and, thus, a convergence of waves will constructively interfere at the location of the microphone. The resulting superposition of the focusing produced by each of the eight sources broadcasting their TRIR signals is recorded at the focal position by the microphone. This focusing of sound is repeated with different levels of amplification, and these focal signals are linearly scaled and compared to look for differences as the input amplitudes are increased [examples shown in Figs. 2(c) and 2(d) with different zoom levels]. Note that it is hard to compare what amplitude features are changing in these focal signals, as the input voltage amplitude is increased. In Sec. III, we will linearly scale these signals.

With that process in mind, the following settings were used. The chirp signal had a length of 4.16 s with 0.34 s of trailing zeroes to allow ample time for the reverberation to dampen in preparation for the broadcast of the chirp signal from the next driver. The frequency progression in the chirp was logarithmic to match that of Patchett and Anderson<sup>2</sup> and had a bandwidth of 500-3500 Hz due to the limitations mentioned previously. A sampling frequency of 250 kHz is used both for the generation of the signals and their recording. The chirp signals are output from the sound card with a peak amplitude of 100 mV into the amplifier. The amplitude of signals output from the sound cards and input to the amplifier will thus be called an input amplitude. After the CRs are recorded and processed into the eight individual TRIRs, we are ready to take the measurements needed. Note that we ensured that the CRs were recorded at sound levels that were amplitude-independent, meaning they were recorded at linear sound levels, and thus, nonlinear content should not be present in these recordings. The sound cards

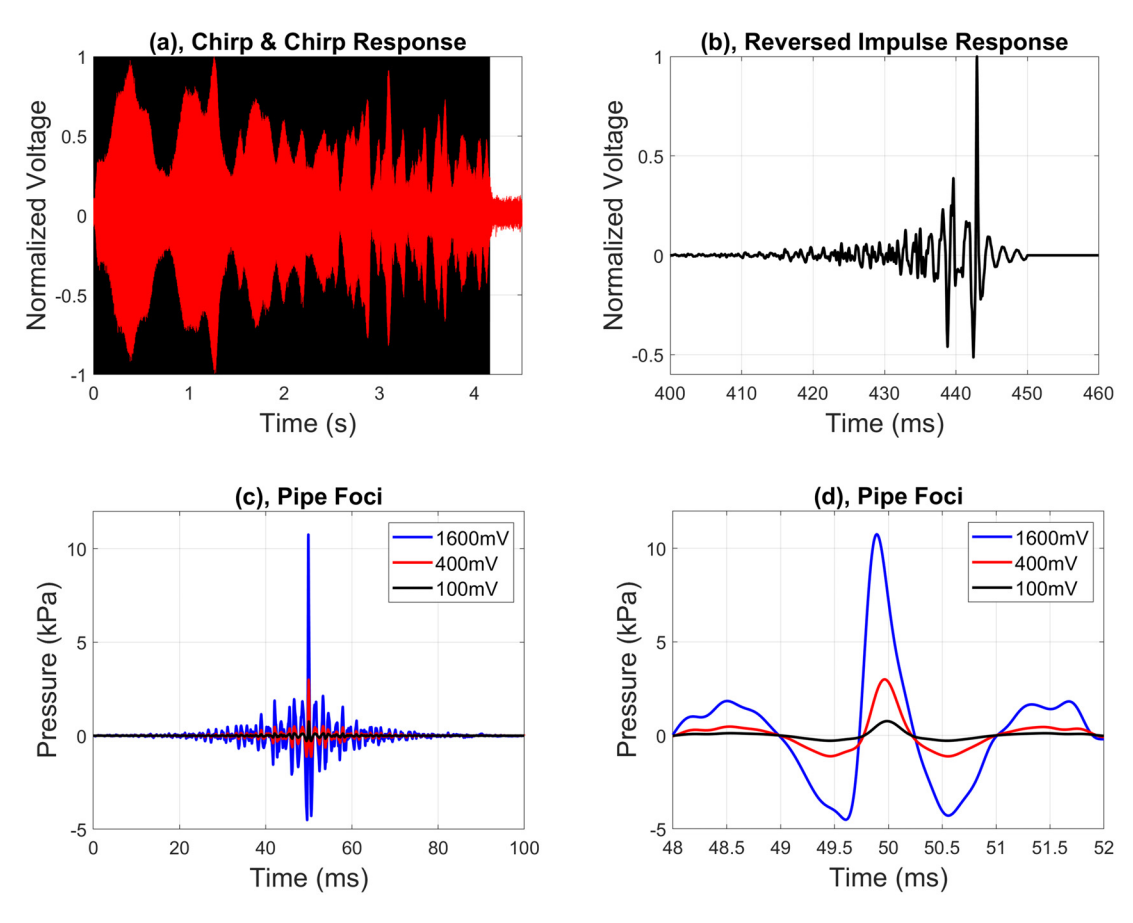


FIG. 2. Example signals used in the TR process for the experiments in the pipes. (a) The chirp source signal (black colored signal) and an example response (red colored signal) to that chirp recording during the forward step. (b) An example TRIR. (c) Focal signals recorded during the backward step due to three different input voltage amplitudes. (d) Zoomed in version of (c).

can generate output amplitudes of  $100-1800\,\mathrm{mV}$ , and it was determined to use 3 dB increases for the input amplitude levels (multiplying the previous input level by  $\sqrt{2}$ ) beginning at  $100\,\mathrm{mV}$  and stopping at  $1600\,\mathrm{mV}$ . This produces nine increasing levels of output from the audio cards ( $100\,\mathrm{mV}$ ,  $141\,\mathrm{mV}$ ,  $200\,\mathrm{mV}$ ,  $282\,\mathrm{mV}$ ,  $400\,\mathrm{mV}$ ,  $565\,\mathrm{mV}$ ,  $800\,\mathrm{mV}$ ,  $1131\,\mathrm{mV}$ , and  $1600\,\mathrm{mV}$ ).

It should be noted that there were a lot of preliminary experiments that were conducted prior to settling on the settings mentioned. The amplifier settings and input voltage range were optimized to create the TR foci in such a way to make sure that our range of experiments transitioned from the limits of the linear range to when the focusing was loud enough to visibly observe nonlinear features. The chirp signal was broadcast at several output amplitudes to verify that the CR signals we were recording were still within the linear regime (there was no apparent distortion of the signals as a function of amplitude). It was desired to broadcast the chirp signals at a high enough amplitude to attain a good signal to noise ratio but low enough to avoid nonlinear wave propagation during the forward step. Two different kinds of microphones [different makes and models and different transduction mechanisms (condenser versus piezoelectric)] were placed end to end, including the one used in the presented experiments, to confirm that both microphones were recording the same waveforms and that there was no visible distortion caused by the microphone itself. A lot of additional experiments were done to find out how best to hold the microphone inside the pipe before settling on the description we previously described.

It is worth noting that a few different pipe configurations were also tested to ensure that our specific setup used is not affecting our conclusions. Some experiments were conducted in a 1.60 m long straight pipe with a driver on each end. A microphone was again placed inside the pipe. The same types of nonlinear features were present in these focal signals, though to a lesser extent because we were only utilizing two drivers. It was decided that eight drivers be used to generate larger amplitudes, and in order to allow eight drivers to all broadcast sound into a 1-D pipe system, we had to introduce three- and four-way pipe branches.

For comparison to the pipe system, a classical TR experiment was done inside the small reverberation chamber at Brigham Young University. This reverberation chamber has dimensions  $5.7 \text{ m} \times 4.3 \text{ m} \times 2.5 \text{ m}$ . The overall reverberation time in the room is approximately  $3.16 \pm 0.08$  s across the chirp bandwidth used, and the room has a Schroeder frequency of 522 Hz. The physical setup matches the setup of Patchett and Anderson. 22 This includes the drivers being mounted to horns and facing them away from the microphone,<sup>53</sup> which was placed in a corner of the room.<sup>54</sup> The same bandwidth of 500-3500 Hz and input amplitudes are used in the room experiments as in the pipe experiments except for the trailing zeroes length being longer at 3.84 s to account for the longer reverberation time in the room. The reverberation times in the two systems are thus very different. However, the authors are unaware of any amplitude

dependent effects that would be impacted by differing reverberation times (certainly not any that would cause a nonlinear increase in compression amplitudes due to inclusion of longer reverberation times in the room). Waves in the pipe system do not travel as far as they do in the room, and there is clearly more attenuation of waves traveling in the pipe system. Thus, while there are differences in the two systems, the authors assert that the most important consideration is that the amplitudes at the time of focusing are similar in the two systems.

Note that for both sets of experiments, the recordings of the TR focusing by the microphone were low-pass filtered with a cutoff frequency of 3500 Hz, during post processing, in order to ensure that only plane waves were used in the analysis. This eliminates waves that may travel as crossmodes in the pipe system that may have been generated by amplifier distortion. Since the bandwidth used spans from 500 to 3500 Hz, integer multiple harmonics of frequencies between 500 and 1750 Hz could remain in the measured signals even after the low-pass filter is applied. Thus, some nonlinear wave steepening, which causes harmonic generation in the propagation of finite amplitude waves, will still be observable.

The TR focusing at 100 mV was repeated ten times in order to estimate the uncertainty of our measurements. The average peak pressure amplitude of TR focusing in the pipe system was 760.04 Pa (corresponding to a peak sound pressure level of 151.6 dB re  $20 \mu Pa$ ). The standard deviation among these peak pressures over the ten repetitions of the experiment was 0.12 Pa. Then, with the horns receiving no input voltage, the background root mean square (RMS) pressure amplitude averaged 1.98 Pa over the signal length, and thus the signal to noise ratio (comparing the peak amplitude of the focusing with 100 mV input voltage to the background RMS pressure amplitude) was approximately 52 dB. The peak amplitude of the TR focusing with 1600 mV input voltage was 10748 Pa (corresponding to a peak sound pressure level of 174.6 dB re 20 μPa), yielding a maximum signal to noise ratio of about 75 dB.

#### III. RESULTS

To allow a linear scaling analysis, <sup>55</sup> each TR focal signal was multiplied by a scaling factor, *S*,

$$S = \frac{1600}{I},\tag{2}$$

where *I* is the input amplitude in mV generated from the sound cards. For linear cases, this would generate copies of the highest amplitude signal. If nonlinearities are present, the scaling factor allows identification of differences between the results of using lower amplitude inputs and higher amplitude inputs to the system. Figure 3(b) shows example results from three superimposed TR focal signals recorded when performing TR in the 1-D pipe system, with each input amplitude spaced by 12 dB. We observe that as the input amplitude increases, the scaled peak compression

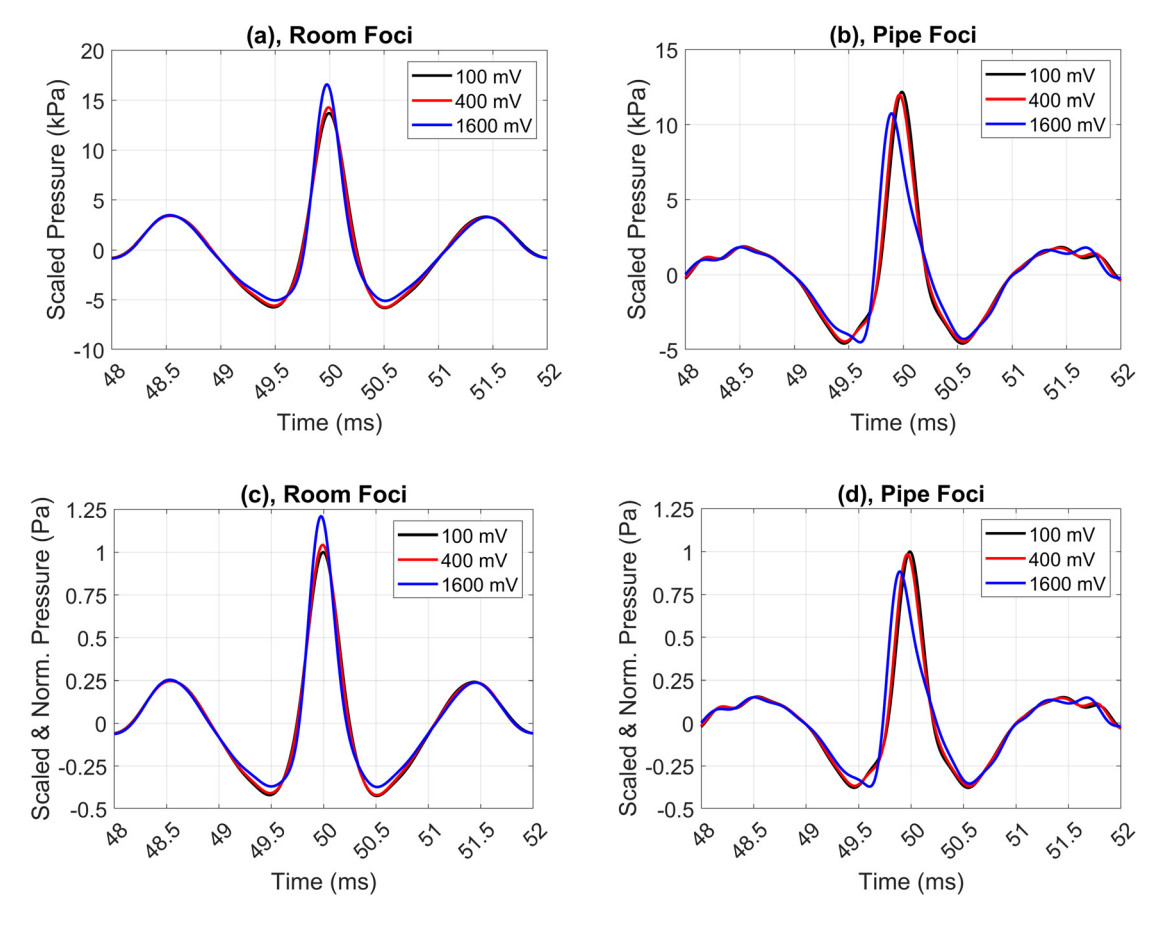


FIG. 3. (a) Scaled TR focal signals when focusing 3-D sound within a room. Note the increase in scaled peak compression amplitude and earlier arrivals of the peak compression. (b) Scaled TR focal signals when focusing 1-D sound within pipes. Note the decrease in scaled peak compression amplitudes and earlier arrivals of the peak compression. The pressure values in kPa are accurate for the 1600 mV plots, and the values for the 100 mV plots can be found by dividing the numbers shown in kPa by 16 and the values for the 400 mV plots can be found by dividing by 4. The plots in (c) and (d) show the same data as in (a) and (b), respectively, but they have been normalized with respect to the peak amplitudes of the respective 100 mV signals.

amplitude decreases. This indicates a nonlinear suppression of compressions as the amplitude from the drivers increases. Notably, this finding is contrary to the findings of Willardson et al.21 and Patchett and Anderson,22 whose experiments were done with 3-D wave focusing in a room, but was expected here since this experiment is done solely with 1-D waves, where Mach stems are not expected to form. Additionally, the higher amplitude focus peak arrives earlier in time with a steepening of the leading edge of the wave, indicating waveform steepening. This coincides with the claims of Willardson et al., 21 Patchett and Anderson, 22 and Patchett et al., 23 who all asserted that waveform steepening is present in higher amplitude focal signals. The results shown in Fig. 3(b) are exemplary of many experiments done at various amplitudes within the pipes under various conditions.

With these linearly scaled plots in Figs. 3(a) and 3(b), one can easily see how the progressively higher amplitude results deviate from the lowest amplitude result (which would have the least amount of nonlinearity impacting this result). Note that the first large rarefaction shown in Fig. 3(b) arrives noticeably later in time for the 1600 mV result than it does for the 100 mV result (it arrives slightly later for

the 400 mV result). The largest compression peak arrives noticeably earlier for the 1600 mV result than for the 100 mV result (and slightly earlier for the 400 mV result). This compression peak is also lower in amplitude for the 1600 mV and 400 mV results than for the 100 mV result. The leading edge of the main compression peak is also steeper for the 1600 mV result than for the 100 mV result. When finite amplitude waves propagate, it is well known that rarefactions travel slower than the linear speed of sound and that compressions travel faster, leading to waveform steepening. It is also well known that the peaks and troughs of a finite amplitude wave can decrease in magnitude as they travel. Note that the compression at 48.5 ms arrives at the same time, irrespective of amplitude and that the amplitude of this peak linearly scales, and thus, we can assert that there are no noticeable nonlinear wave propagation effects for that peak due to its lower amplitude.

These TR focusing results in the pipes are now contrasted with TR focusing results obtained in a room using similar settings (the microphone was placed in a corner of the room as was done by Patchett and Anderson<sup>22</sup>). Figure 3(a) shows TR focal signals when using the same input amplitudes in a room as used in the pipes. Similar features as those

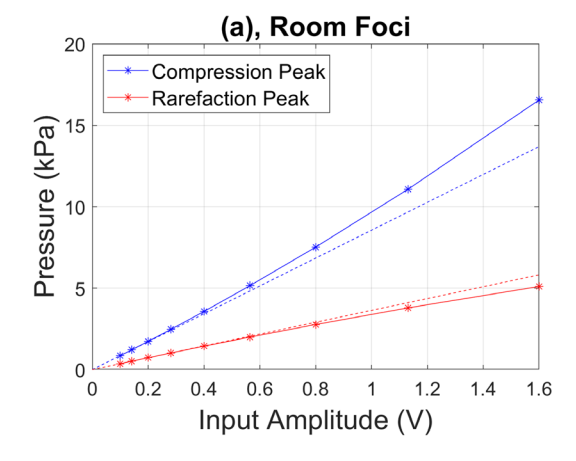
reported by Patchett and Anderson<sup>22</sup> are observed; namely, as the amplitude from the drivers increases, a nonlinear increase in the peak compression amplitude is observed (nonlinear amplification) along with a nonlinear suppression of the rarefactions on either side of that main focal peak. Steepening of the waveform is also observed, though it is harder to observe here. The key difference between these two sets of results is the 1-D environment for the pipes and the 3-D environment for the room. The nonlinear amplification of peak compression and nonlinear suppression of the adjacent rarefactions was also reported by Willardson et al.21 and by Patchett and Anderson<sup>22</sup> though here a narrower bandwidth of frequencies was used. Willardson et al.<sup>21</sup> and Patchett and Anderson<sup>22</sup> claimed these features were the result of Mach stem formation with the overlapping of high-pressure waves. Patchett et al.<sup>23</sup> showed through numerical modeling that indeed Mach stem formation in collapsing waves allows additional energy to arrive at the time of maximal focusing causing the nonlinear amplification of compressions.

Figures 3(c) and 3(d) display the same data as found in Figs. 3(a) and 3(b), but the data has been normalized with respect to the peaks of the respective 100 mV signals. This allows visual identification of the fractional increases in amplitude of the compression peaks as the input voltage amplitude is increased for the room foci [Fig. 3(c)] and the fractional decreases in amplitude of the compression peaks as the input voltage amplitude is increased for the pipe foci [Fig. 3(d)].

We show further that as the input amplitude increases, we depart further from linearity. Figure 3 shows the peak amplitudes of the main focal compressions and the peak amplitudes of the largest rarefactions for various input amplitudes (the solid lines with the markers) as compared to linear scaling (the dotted lines) of the peak compression and rarefaction pressures that the 100 mV input creates. It is clear that there is a nonlinear suppression of the higher amplitudes for both the compressions and rarefactions. The nonlinear suppression of the rarefaction amplitude is consistent with what is found by Patchett and Anderson, <sup>22</sup> but the compression amplitude progression shows the opposite

here; a decrease relative to linear scaling is observed in pipes rather than a nonlinear increase in peak compression pressures in rooms as input amplitude increases. Compare Fig. 4 here to Fig. 9 in Patchett and Anderson. The peak pressure level of the maximum of the TR focusing within the room system for the  $100\,\mathrm{mV}$  input was  $855.82\,\mathrm{Pa}$  (corresponding to a peak sound pressure level of  $152.6\,\mathrm{dB}$  re  $20\,\mu\mathrm{Pa}$ ) and the peak pressure for the  $1600\,\mathrm{mV}$  input was  $16\,551\,\mathrm{Pa}$  (corresponding to a peak sound pressure level of  $178.4\,\mathrm{dB}$  re  $20\,\mu\mathrm{Pa}$ ). Thus, the peak levels for the pipe system span from  $151.6\,\mathrm{dB}$  to  $174.6\,\mathrm{dB}$ , whereas the peak levels in the room span from  $152.6\,\mathrm{dB}$  to  $178.4\,\mathrm{dB}$ .

Figure 5(a) shows example focal signals for the minimum and maximum input voltages. Additional lines have been drawn on this figure to aid in quantifying metrics related to nonlinearity exhibited in the focal signals as a function of input voltage. The difference in the scaled, peak compression amplitudes is apparent in this figure. The variation of these peak amplitudes is shown as a function of input voltage in Fig. 5(b). As noted previously, the peak amplitudes nonlinearly increase in the room and nonlinearly suppress in the pipes with increasing input voltage. Along with the nonlinear suppression, we observe an increase in the wave steepening of the leading edge of the main compression peak as quantified by the maximum slope/derivative, which is to say that steepening increases with increasing input amplitude. Consistent with wave steepening effects, the peak compressions arrive progressively earlier with increasing input amplitude. In Fig. 5(a), the arrival times are denoted by vertical lines, and the variation as a function of input amplitude is shown in Fig. 5(c). Note that the variation in the arrival times is more dramatic in the pipes than in the room. The earlier arrival of the peaks in the room results is consistent with Patchett and Anderson's findings.<sup>22</sup> This effect is more pronounced in the pipes, as nonlinearities are more easily generated (the shock formation distance is shorter) in 1-D propagation (focusing of waves in a pipe) than in 3-D propagation (focusing of waves in a room).<sup>31</sup> In Fig. 5(a), the maximum derivative of each signal is denoted



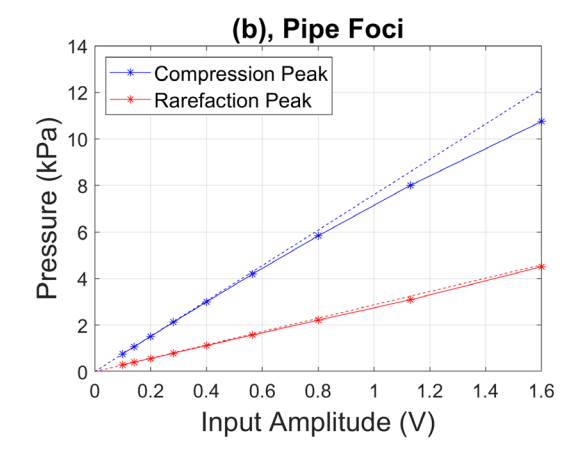


FIG. 4. Peak amplitudes of the primary compression of the TR focus and the peak amplitudes of the largest rarefaction shown at each of nine input amplitudes as compared with the linear case (extrapolating linearly from the lowest amplitude). (a) 3-D focusing of sound in a room. (b) 1-D focusing of sound in pipes.

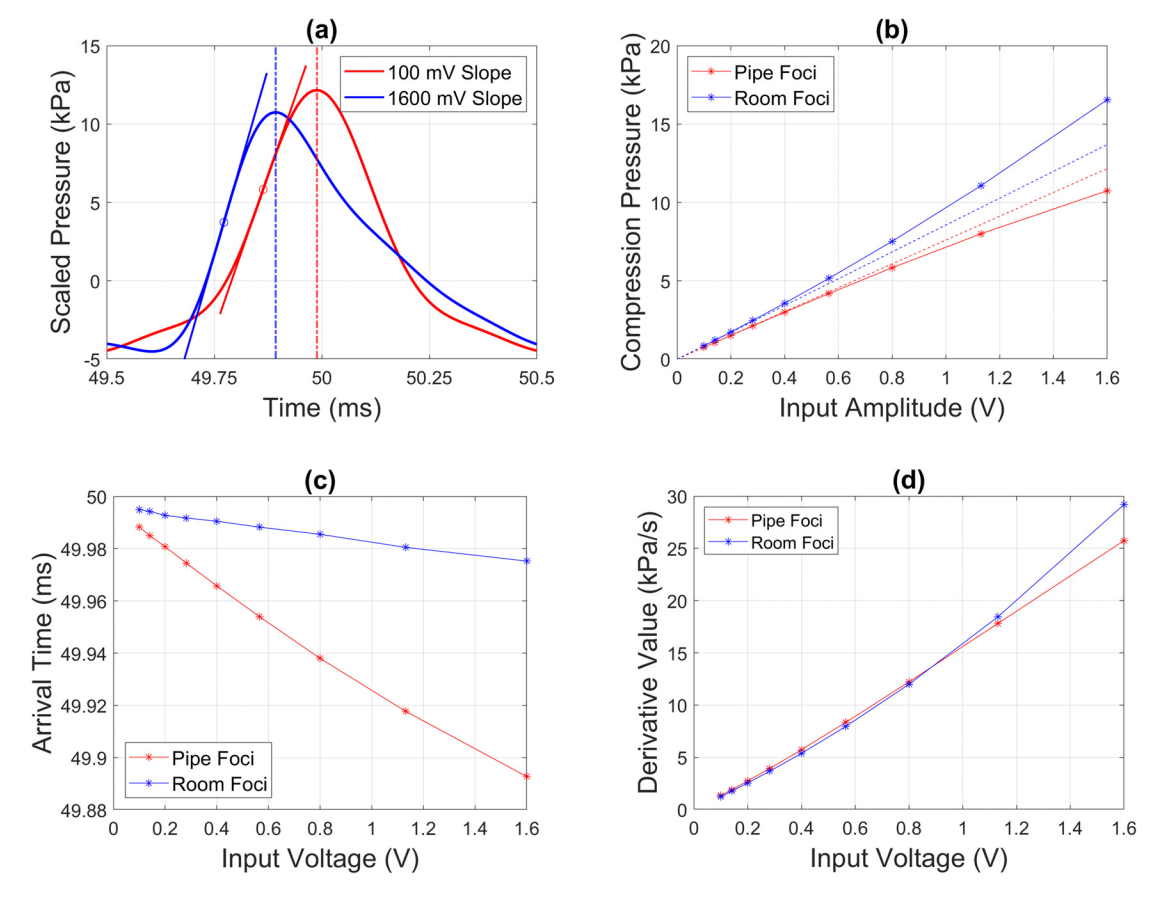


FIG. 5. (a) Low and high amplitude focal signals are compared. The maximum derivative of the leading edge of the main compression peak in each focal signal is denoted by circles with tangent lines that possess the respective maximum slopes. The vertical, dashed-dotted lines denote the time of maximum compression amplitude for each focal signal. (b) Peak compression amplitudes of TR focusing in pipes and in the room, which data is shown in Fig. 4. (c) Arrival times for the peak compression amplitudes in pipes and in the room.

by a circle with a tangent line drawn. In Fig. 5(d), the variation of maximum derivative is shown as a function of input amplitude, with a minor difference between the data in the pipes and in the room at the highest amplitudes. If everything scaled linearly in these two experiments, then no nonlinear amplification or suppression of the main compression peaks would be observed. The arrival times of the peak compressions would not change, and the derivatives of the leading edge of the compression would not change either.

#### IV. CONCLUSION

In this environment where only 1-D plane waves may propagate, high amplitude TR focusing yields a nonlinear suppression or decrease in the peak compression amplitude as the input amplitude is increased. In addition, it was found that the peak compression of the focusing arrives earlier in time and has a higher valued slope/derivative of the leading edge of the main focal compression. These effects are consistent with the ideas of waveform steepening leading to shock wave formation. By restricting the wave propagation to 1-D plane waves in the pipe system, the potential for Mach stem formations is eliminated and no nonlinear amplification of the compression amplitude is observed. The amplitude of the TR focusing in the pipes here is within the

amplitude range explored for TR focusing in rooms, but a major difference between the two experiments is the 1-D propagation of plane waves in the pipes and the 3-D propagation of spherical waves in the room (the formation of Mach stems, with one wave catching up to another, requires curvature of nearly overlapping wavefronts). This experimental finding is consistent with the Mach stem explanation for the nonlinear amplification reported by Willardson *et al.*<sup>21</sup> and Patchett and Anderson<sup>22</sup> and explored through numerical simulations by Patchett *et al.*<sup>23</sup>

#### **ACKNOWLEDGMENTS**

Funding provided by the BYU College of Computational, Mathematical, and Physical Sciences.

### AUTHOR DECLARATIONS Conflict of Interest

The authors have no conflicts of interest to disclose.

#### **DATA AVAILABILITY**

The data that support the findings of this study are available from the corresponding author upon reasonable request.

## JASA

#### https://doi.org/10.1121/10.0039638

- <sup>1</sup>M. Fink, "Time reversed acoustics," Phys. Today **50**(3), 34–40 (1997).
- <sup>2</sup>B. E. Anderson, M. Griffa, P. A. Johnson, C. Larmat, and T. J. Ulrich, "Time reversal," Acoust. Today 4(1), 5–16 (2008).
- <sup>3</sup>B. E. Anderson, M. C. Remillieux, P.-Y. Le Bas, and T. J. Ulrich, "Time reversal techniques," in *Nonlinear Acoustic Techniques for Nondestructive Evaluation*, 1st ed., edited by T. Kundu (Springer, New York, 2019), pp. 547–581.
- <sup>4</sup>B. E. Anderson, "High amplitude time reversal focusing of sound and vibration," Proc. Mtgs. Acoust. **51**, 032001 (2023).
- <sup>5</sup>A. Parvulescu and C. Clay, "Reproducibility of signal transmissions in the ocean," Radio Electron. Eng. U.K. **29**(4), 223–228 (1965).
- <sup>6</sup>C. S. Clay and B. Anderson, "Matched signals: The beginnings of time reversal," Proc. Mtgs. Acoust. **12**, 055001 (2011).
- <sup>7</sup>H. C. Song, "An overview of underwater time-reversal communication," IEEE J. Oceanic Eng. **41**(3), 644–655 (2016).
- <sup>8</sup>H. C. Song, G. Byun, and J. S. Kim, "Remote acoustic illumination using time reversal and a surface ship," J. Acoust. Soc. Am. **145**(3), 1565–1568 (2019).
- <sup>9</sup>B. E. Anderson, T. J. Ulrich, P.-Y. Le Bas, and J. A. Ten Cate, "Three-dimensional time reversal communications in elastic media," J. Acoust. Soc. Am. **139**(2), EL25–EL30 (2016).
- <sup>10</sup>C. S. Larmat, R. A. Guyer, and P. A. Johnson, "Time-reversal methods in geophysics," Phys. Today 63(8), 31–35 (2010).
- <sup>11</sup>S. Cheinet, L. Ehrhardt, and T. Broglin, "Impulse source localization in an urban environment: Time reversal versus time matching," J. Acoust. Soc. Am. 139(1), 128–140 (2016).
- <sup>12</sup>A. Mimani, Z. Prime, D. J. Moreau, and C. J. Doolan, "An experimental application of aeroacoustic time-reversal to the Aeolian tone," J. Acoust. Soc. Am. 139(2), 740–763 (2016).
- <sup>13</sup>B. E. Anderson, M. Griffa, T. J. Ulrich, P.-Y. Le Bas, R. A. Guyer, and P. A. Johnson, "Crack localization and characterization in solid media using time reversal techniques," in *Proceedings of the 44th U.S. Rock Mechanics Symposium and 5th U.S.-Canada Rock Mechanics Symposium*, Salt Lake City, UT (2010).
- <sup>14</sup>S. M. Young, B. E. Anderson, S. M. Hogg, P.-Y. Le Bas, and M. C. Remillieux, "Nonlinearity from stress corrosion cracking as a function of chloride exposure time using the time reversed elastic nonlinearity diagnostic," J. Acoust. Soc. Am. 145(1), 382–391 (2019).
- <sup>15</sup>P.-Y. Le Bas, M. C. Remillieux, L. Pieczonka, J. A. Ten Cate, B. E. Anderson, and T. J. Ulrich, "Damage imaging in a laminated composite plate using an air-coupled time reversal mirror," Appl. Phys. Lett. 107, 184102 (2015).
- <sup>16</sup>M. Farin, C. Prada, T. Lhommeau, M. El Badaoui, and J. de Rosny, "Towards a remote inspection of jet engine blades using time reversal," J. Sound Vib. 525, 116781 (2022).
- <sup>17</sup>R. S. Russell, B. E. Anderson, and M. H. Denison, "Using time reversal with long duration broadband noise signals to achieve high amplitude and a desired spectrum at a target location," Appl. Acoust. 236, 110744 (2025).
- <sup>18</sup>J.-L. Thomas, F. Wu, and M. Fink, "Time reversal focusing applied to lithotripsy," Ultrason. Imaging 18(2), 106–121 (1996).
- <sup>19</sup>M. Tanter, J.-L. Thomas, and M. Fink, "Focusing and steering through absorbing and aberrating layers: Application to ultrasonic propagation through the skull," J. Acoust. Soc. Am. 103(5), 2403–2410 (1998).
- <sup>20</sup>J.-L. Thomas and M. Fink, "Ultrasonic beam focusing through tissue inhomogeneities with a time reversal mirror: Application to transskull therapy," IEEE Trans. Ultrason, Ferroelect, Freq. Contr. 43(6), 1122–1129 (1996).
- <sup>21</sup>M. L. Willardson, B. E. Anderson, S. M. Young, M. H. Denison, and B. D. Patchett, "Time reversal focusing of high amplitude sound in a reverberation chamber," J. Acoust. Soc. Am. 143(2), 696–705 (2018).
- <sup>22</sup>B. D. Patchett and B. E. Anderson, "Nonlinear characteristics of high amplitude focusing using time reversal in a reverberation chamber," J. Acoust. Soc. Am. 151(6), 3603–3614 (2022).
- <sup>23</sup>B. D. Patchett, B. E. Anderson, and A. D. Kingsley, "Numerical modeling of Mach-stem formation in high-amplitude time-reversal focusing," J. Acoust. Soc. Am. 153(5), 2724–2732 (2023).
- <sup>24</sup>B. E. Anderson, T. J. Ulrich, and P.-Y. Le Bas, "Comparison and visualization of focusing wave fields of various time reversal techniques in elastic media," J. Acoust. Soc. Am. 134(6), EL527–EL533 (2013).
- <sup>25</sup>T. J. Ulrich, P. A. Johnson, and A. Sutin, "Imaging nonlinear scatterers applying the time reversal mirror," J. Acoust. Soc. Am. 119(3), 1514–1518 (2006).

- <sup>26</sup>T. J. Ulrich, A. M. Sutin, T. Claytor, P. Papin, P.-Y. Le Bas, and J. A. TenCate, "The time reversed elastic nonlinearity diagnostic applied to evaluation of diffusion bonds," Appl. Phys. Lett 93(15), 151914 (2008).
- <sup>27</sup>S. Dos Santos and Z. Prevorovsky, "Imaging of human tooth using ultrasound based chirp-coded nonlinear time reversal acoustics," Ultrasonics 51(6), 667–674 (2011).
- <sup>28</sup>C. B. Wallace and B. E. Anderson, "High-amplitude time reversal focusing of airborne ultrasound to generate a focused nonlinear difference frequency," J. Acoust. Soc. Am. 150(2), 1411–1423 (2021).
- <sup>29</sup>M. S. Canney, M. R. Bailey, L. A. Crum, V. A. Khokhlova, and O. A. Sapozhnikov, "Acoustic characterization of high intensity focused ultrasound fields: A combined measurement and modeling approach," J. Acoust. Soc. Am. 124(4), 2406–2420 (2008).
- <sup>30</sup>S. L. Garrett, *Understanding Acoustics*, 2nd ed. (Springer, New York, 2020), pp. 358–373.
- <sup>31</sup>M. F. Hamilton and D. T. Blackstock, *Nonlinear Acoustics* (Springer, Cham, Switzerland, 2024), Chap. 1, Sec. 4.5.4.2.
- <sup>32</sup>A. L. Thuras, R. T. Jenkins, and H. T. O'Neil, "Extraneous frequencies generated in air carrying intense sound waves," J. Acoust. Soc. Am. 6, 173–180 (1935).
- <sup>33</sup>S. H. Burns, "Finite-amplitude distortion in air at high acoustic pressures," J. Acoust. Soc. Am. 41(4), 1157–1169 (1967).
- <sup>34</sup>D. F. Pernet and R. C. Payne, "Non-linear propagation of signals in air," J. Sound Vib. 17(3), 383–396 (1971).
- <sup>35</sup>F. M. Pestorius, "Propagation of plane acoustic noise of finite amplitude," Technical Report No. ARL-TR-73-23, Applied Research Laboratories at The University of Texas at Austin, Austin, TX (1973).
- <sup>36</sup>F. M. Pestorius and D. T. Blackstock, "Propagation of finite-amplitude noise," in *Finite-Amplitude Wave Effects in Fluids*, edited by L. Bjorno (IPC Science and Technology Press, Guildford, Surrey, UK, 1973), pp. 24–29.
- <sup>37</sup>L. E. Falco, "Single-point nonlinearity indicators for the propagations of high-amplitude acoustic signals," Ph.D. dissertation, The Pennsylvania State University, University Park, PA, 2007.
- <sup>38</sup>M. B. Muhlestein, "Analyses of nonlinearity measures in high-amplitude sound propagation," M.S. thesis, Brigham Young University, Provo, UT, 2013.
- <sup>39</sup>G. Ben-Dor, Shock Wave Reflection Phenomena (Springer Verlag, New York, 1992), pp. 3–13.
- <sup>40</sup>M. M. Karzova, V. A. Khokhlova, E. Salze, S. Ollivier, and P. Blanc-Benon, "Mach stem formation in reflection and focusing of weak shock acoustic pulses," J. Acoust. Soc. Am. 137, EL436–EL442 (2015).
- <sup>41</sup>J. N. Tjøtta and S. Tjøtta, "Nonlinear equations of acoustics, with application to parametric acoustic arrays," J. Acoust. Soc. Am. 69(6), 1644–1652 (1981).
- <sup>42</sup>E. C. Hansen, A. Frank, P. Hartigan, and K. Yirak, "Numerical simulations of Mach stem formation via intersecting bow shocks," High Energy Density Phys. 17, 135–139 (2015).
- <sup>43</sup>G. Montaldo, P. Roux, A. Derode, C. Negreira, and M. Fink, "Ultrasound shock wave generator with one-bit time reversal in a dispersive medium, application to lithotripsy," Appl. Phys. Lett. 80, 897–899 (2002).
- <sup>44</sup>B. D. Patchett, "Focusing of High-Amplitude sound waves using the time reversal process," Ph.D. dissertation, Brigham Young University, Provo, UT, 2022.
- <sup>45</sup>S. Félix and V. Pagneux, "Sound propagation in rigid bends: A multi-modal approach," J. Acoust. Soc. Am. 110(3), 1329–1337 (2001).
- <sup>46</sup>M. Calton, "Modeling of acoustic resonators and resonator systems for use in passive noise control," Masters thesis, Brigham Young University, Provo, UT, 2016.
- <sup>47</sup>ASTM E1050-24: Standard Test Method for Impedance and Absorption of Acoustical Materials Using a Tube, Two Microphones and a Digital Frequency Analysis System (American Society for Testing and Materials, West Conshohocken, PA, 2024).
- <sup>48</sup>ASTM E2611-24: Standard Test Method for Normal Incidence Determination of Porous Material Acoustical Properties Based on the Transfer Matrix Method (American Society for Testing and Materials, West Conshohocken, PA, 2024).
- <sup>49</sup> A. D. Kingsley, J. M. Clift, B. E. Anderson, J. E. Ellsworth, T. J. Ulrich, and P.-Y. Le Bas, "Development of software for performing acoustic time reversal with multiple inputs and outputs," Proc. Mtgs. Acoust. 46, 055003 (2022).

#### https://doi.org/10.1121/10.0039638

JASA

<sup>50</sup>A. D. Pierce, Acoustics: An Introduction to Its Physical Principles and Applications, 3rd ed. (Springer, New York, 2019), pp. 363–365.

<sup>51</sup>E. D. Golightly, B. E. Anderson, A. D. Kingsley, R. Russell, and R. Higgins, "Super resolution, time reversal focusing using path extending properties of scatterers," Appl. Acoust. 206, 109308 (2023).

<sup>52</sup>B. Van Damme, K. Van Den Abeele, Y. Li, and O. Bou Matar, "Time reversed acoustics techniques for elastic imaging in reverberant and non-reverberant media: An experimental study of the chaotic cavity transducer concept," J. Appl. Phys. 109, 104910 (2011).

<sup>53</sup>B. E. Anderson, M. Clemens, and M. L. Willardson, "The effect of transducer directivity on time reversal focusing," J. Acoust. Soc. Am. 142(1), EL95–EL101 (2017).

<sup>54</sup>B. D. Patchett, B. E. Anderson, and A. D. Kingsley, "The impact of room location on time reversal focusing amplitudes," J. Acoust. Soc. Am. 150(2), 1424–1433 (2021).

<sup>55</sup>M. Scalerandi, A. S. Gliozzi, C. L. E. Bruno, D. Masera, and P. Bocca, "A scaling method to enhance detection of a nonlinear elastic response," Appl. Phys. Lett. 92(10), 101912 (2008).